ELSEVIER

Contents lists available at ScienceDirect

#### Construction and Building Materials

journal homepage: www.elsevier.com/locate/conbuildmat





## Reducing the cracking potential of ultra-high-performance concrete (UHPC) with the prewet expansive agent

Jiang Du<sup>a,b</sup>, Xiao Tan<sup>a</sup>, Yuhuan Wang<sup>a</sup>, Yi Bao<sup>a</sup>, Weina Meng<sup>a,\*</sup>

- a Department of Civil, Environmental and Ocean Engineering, Stevens Institute of Technology, Hoboken, NJ, USA
- b State Key Laboratory of Mountain Bridge and Tunnel Engineering, Chongqing Jiaotong University, Chongqing 400074, People's Republic of China

#### ARTICLE INFO

# Keywords: Ultra-high-performance concrete CaO-type expansive agent Prewet time Autogenous shrinkage Cracking potential

#### ABSTRACT

With superior mechanical strength and durability, ultra-high-performance concrete (UHPC) is becoming an emerging material for resilient infrastructures. However, due to its high shrinkage, the high early-age cracking potential hinders its promotion. The expansive agent (EA) is therefore intensively used to reduce the shrinkage. However, the insufficient free water and dense microstructure of UHPC limit its expansion effect, thus affecting EA's capacity on shrinkage reduction and cracking control. To achieve the minimum cracking potential of UHPC, the CaO-type EA was prewet with mixing water before concrete batching. Results indicated that, after 45-min premix treatment, the 4% prewet EA compare to the 4% EA without prewet, shown: (1) increase in 3-day and 28-day splitting tensile strengths of UHPC by up to 10% and 5%; (2) reduction in 3-day and 28-day autogenous shrinkage of UHPC by around 20% and up to 30%; (3) reduction in the peak and cumulative cracking potential of UHPC by up to 30% and 25%. The prewet process of CaO-type EA was proven to efficiently increase the content of expansive products in UHPC, which contributes to reducing the autogenous shrinkage and increasing tensile strengths, therefore significantly enhancing the cracking resistance, especially at early ages.

#### 1. Introduction

Ultra-high-performance concrete (UHPC) is an advanced class of cementitious composites that has self-consolidating property, superior mechanical performance, and excellent durability [1,2]. Therefore, UHPC has been used in some infrastructure, like precast girder [3–5], field-cast connections and joints [6–9], jackets for columns [10], bridge deck overlay [11–16], and reinforcement of damaged bridge arches [17–19]. However, UHPC typically exhibits significant autogenous shrinkage (>500  $\,\mu e$  at 3 days) due to its high binder content (>1200 kg/m³), absence of coarse aggregates, and low water-to-binder ratio (0.15–0.23), leading to early-age cracking or debonding. Any damage will significantly affect the durability of the infrastructure. Therefore, to mitigate the shrinkage and reduce the cracking potential of UHPC are critical to extend the service life of the infrastructure [20].

Autogenous shrinkage of UHPC is due to the self-desiccation effect and chemical shrinkage due to cement hydration [21], which contributes to the majority of total shrinkage in UHPC [22–24]. Traditionally, the reduction of cement pastes is the major solution to control the shrinkage [25]. Plenty of mitigation methods were investigated in the past few years [26]: (1) control cement hydration by replacing the

cement with supplementary cementitious materials (SCMs) [27–29]; (2) add internal restraint through incorporating coarse aggregates [30,31]; (3) reduce pore solution surface tension via using shrinkage reducing agent (SRA) [32,33]; (4) increase the internal relative humidity by employing the internal curing agents (ICA) [1,34]; (5) formation of expansive products by adding expansive agents (EAs) [35,36].

It is noteworthy that the cracking potentials of UHPC is not solely determined by the development of autogenous shrinkage, but also depended on the development of tensile strengths [37]. In comparison, adding EAs is reported to significantly reduce the autogenous shrinkage as well as increase the early-age tensile strength [35], thus minimizing the cracking potentials of UHPC. The underlying mechanism of EA is to gradually form the expansive products, which resists the developed shrinkage stress, thus reducing the autogenous shrinkage, shown in Fig. 1 [38].

However, the use of EAs in UHPC mixtures still has some challenges. The degree of expansion reaction is relatively low and not controllable so that its capacity on the shrinkage mitigation and the cracking control are restrained. The underlying reasons are: (1) due to the low w/b, UHPC has insufficient free water for EA to fully react [39], shown in Fig. 2(a); (2) due to the dense microstructure and the rapid strength

E-mail address: wmeng3@stevens.edu (W. Meng).

<sup>\*</sup> Corresponding author.

The growth of expansive products against shrinkage stress to restrain the autogenous shrinkage

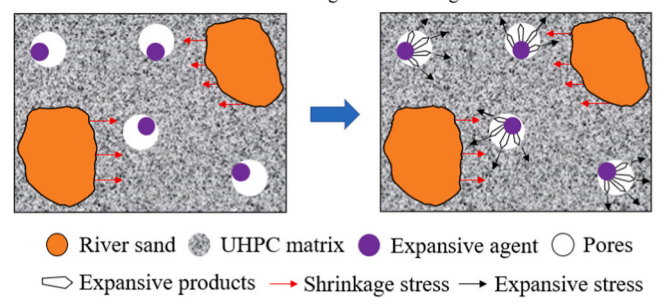


Fig. 1. The underlying mechanism of EA in UHPC.

development, UHPC has extremely limited spaces for expansive products to expand [36], shown in Fig. 2(b). Therefore, more in-depth and comprehensive studies are needed to optimize EA applications in UHPC mixtures.

Three main expansive agents were usually used, including calcium sulfoaluminate (CSA)-type EA [40], calcium oxide (CaO)-type EA, and magnesium oxide (MgO)-type EA [41]. The expansive products of CSA-type EA, CaO-type EA, and MgO-type EA are ettringite, portlandite, and brucite, respectively [26]. Among them, the ettringite generation consumes a large amount of free water so that CSA-type EA is inappropriate to apply in UHPC mixtures since the limited free water restrains the efficiency of the expansion reaction. In addition, the ettringite decomposes over 70 °C, so the expansion effect might disappear when applying heat curing or applying in massive infrastructures [42]. On the other hand, MgO-type EA requires less free water to form the expansion product (i.e., brucite), which is more stable under high temperatures. However, the expansion reactivity of MgO-type EA is relatively low. The rapid strength development of UHPC restrains the reaction of MgO-type EA and the delayed expansion caused by brucite might introduce micro or/and macro cracks, which are harmful for the long-term mechanical performance and the durability of UHPC infrastructure. Therefore, neither CSA-type nor MgO-type EAs are suitable for the UHPC mixtures. In comparison, with the lower free water consumption and the acceptable reactivity, CaO-type EA is more appropriate for the UHPC applications [36]. The expansion reaction between CaO-type EA and free water mainly occurs in the first 1–2 days [36]. For example, Shen et al. [36] found that as the CaO-type EA increased to 5% (by mass of cement), the 7-day autogenous shrinkage of cement pastes with 0.18 w/b was completely eliminated.

However, the excessive EA addition not only retards the increment of

the shrinkage but also undermines mechanical strengths [36,43,44]. For instance, Su et al. [45] revealed that, as CaO-MgO compound EA content increased to 4% (by volume), the 7-day autogenous shrinkage was reduced by 15% but the 7-day compressive strengths were reduced over 20%. The reduction in mechanical properties was attributed to: (1) The excessive EAs addition consumes the high-volume free water for cement reaction [36]; (2) The excessive EAs addition increases the possibility of localized expansion, thus generating the weak zones in UHPC matrix [26]. Therefore, the new processing methods with reduced amount of CaO-type EA should be developed to prevent the degradation of mechanical strength and durability. Specifically, the new processing methods aim to increase the degree of expansion reaction when the EA contents are relatively low. Shen et al. [36] proposed to increase the specific surface area of CaO-type EAs by grounding it from 300 to  $350 \text{ m}^2/\text{kg}$  into a higher Blaine fineness (>  $600 \text{ m}^2/\text{kg}$ ) [36,46,47]. The higher specific surface area improves the reactivity of EAs, thus increasing the degree of expansion reaction. Liu et al. [39] proposed to combine the use of EA, superabsorbent polymer (SAP), and shrinkage-reducing agent (SRA) to increase the degree of expansion reaction. The underlying mechanism is, as an efficient internal curing agent, SAP supplied extra free water for EA reaction. Besides, the polymer of SRA would absorb on the surface of cement particles to retard its hydration, which provided more time and spaces for EA reaction. Therefore, the degree of expansion reaction was increased. However, these methods were complicated and significantly increased the initial cost of UHPC mixtures.

To address the above-mentioned issues of EA in UHPC mixtures, a simple processing method for CaO-type usage method is proposed, that is, to prewet the dry CaO-type EA powder with the mixing water prior to the mixing progress. By this way, the dormant period of EA can be shortened, and the expansion reaction of CaO-type EA will be promoted in UHPC mixtures, and the capacity of CaO-type EA on the autogenous shrinkage reduction and the tensile strength improvement in UHPC will be enhanced, thus achieving the better cracking resistance, especially at early ages.

Therefore, the key purpose of this research is to validate a viable method to promote the expansion reaction of EA in UHPC, thus effectively reducing the cracking potential of UHPC. Specifically, the effect of prewet CaO-type EA and mixing water on key behaviors were studied. The comprehensive laboratory experiments were conducted and the corresponding mechanisms were elaborated: (1) to figure out the influence of CaO-type EA content and prewet time on the performance of different types of low-shrinkage UHPC, including workability, autogenous shrinkage, and mechanical strength; (2) to quantify the effect of the prewet CaO-type EA method on cracking potentials of UHPC; and (3) to clarify the prewet CaO-type EA mechanisms in different types of UHPC.

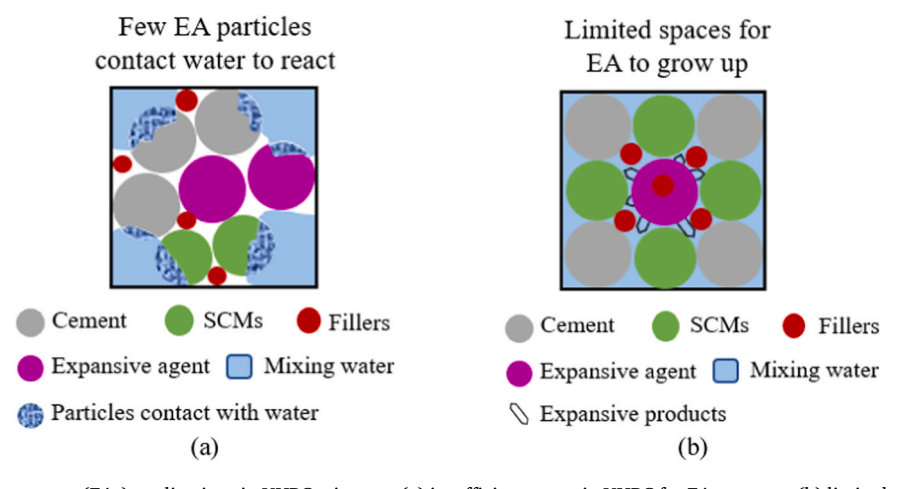


Fig. 2. Challenges of expansive agents (EAs) applications in UHPC mixtures: (a) insufficient water in UHPC for EAs to react; (b) limited spaces for expansive products to grow up.

This research provides a new strategy for improving expansion efficiency of EAs in UHPC and reducing the cracking potentials of UHPC under the restrained conditions.

#### 2. Materials

#### 2.1. Raw materials

Portland cement (Type I) and slag from New Jersey were used as cementitious materials. The CaO-type expansive agent (EA) is a type of dry powder material, and the shrinkage-reducing agent (SRA) consists of an amphiphilic low-molecular-weight polyether. Both were donated by Euclid Chemical to decrease the shrinkage of UHPC. River sand (RS) and porous lightweight sand (LWS) were employed as fine aggregates. The water absorption value of RS and LWS after soaking in water for 24 hours were 0.21% and 17.1%, respectively. The chemical compositions of all dry ingredients were shown in Table 1.

Besides, the distribution curves of dry ingredients particle size are shown in Fig. 3. To enhance the workability and fluidity retention, a polycarboxylate-based high-range water reducer (HRWR) was used. The solid content and specific gravity were 34.4% and 1.05, respectively. Straight steel fibers are also added. The diameter is 0.2 mm, and the length is 13 mm. Besides, the tensile strength and modulus of elasticity are 1.9 GPa and 203 GPa.

#### 2.2. Mixture design

Table 2 shows 11 developed UHPC in this research. The reference mixture was a cost-effective UHPC mixture which was optimized in the previous research based on the performance-based method [27]. The binder-to-sand ratio was 1:1 by volume. The water-to-binder ratio was set at 0.23 by mass. In the test group, seven mixtures (i.e., reference, EA2, EA4, EA6, EA4-P15, EA4-P30, and EA4-P45) were designed to investigate the effect of EA contents and prewet time of EA on the performance of UHPC. Two variables were clearly explained, including the CaO-type EA contents (e.g., 2%, 4%, and 6%, by volume of binders) and prewet time (e.g., 15 min, 30 min, and 45 min). For example, EA4-P15 represents: (1) the CaO-type EA content is 4% by volume of binders; (2) the CaO-type EA is added into the prepared mixing water and prewet for 15 min through the magnetic stirrer.

In addition, the EA was always used in combination with presaturated lightweight sand (LWS) or shrinkage-reducing agents (SRA) to minimize the shrinkage of UHPC mixtures. Hence, four other mixtures (i.e., EA4L25, EA4L25-P45 EA4S2, and EA4S2-P45) in validation groups were designed to further validate the effects of prewet EA by combining

**Table 1**Chemical and physical properties of raw materials.

	Type I Portland cement	Slag	River sand	Lightweight sand
SiO <sub>2</sub> (%)	22.44	36.21	86.50	57.60
Al <sub>2</sub> O <sub>3</sub> (%)	2.76	11.10	0.39	19.40
Fe <sub>2</sub> O <sub>3</sub> (%)	2.24	0.76	1.47	9.60
CaO (%)	68.05	43.75	9.42	3.40
MgO (%)	0.91	5.09	-	2.60
SO <sub>3</sub> (%)	2.25	2.21	-	0.60
Na <sub>2</sub> O (%)	0.19	0.23	-	5.60
K <sub>2</sub> O (%)	0.11	0.40	-	-
TiO <sub>2</sub> (%)	0.14	0.58	-	-
P <sub>2</sub> O <sub>5</sub> (%)	0.09	0.02	-	-
$Mn_2O_3$ (%)	0.03	0.36	-	-
C <sub>3</sub> S (%)	62.35	-	-	-
C <sub>2</sub> S (%)	20.28	-	-	-
C <sub>3</sub> A (%)	1.42	-	-	-
C <sub>4</sub> AF (%)	5.83	-	-	-
Loss on ignition (%)	1.28	0.72	0.24	-
Specific gravity	3.15	2.90	2.64	1.80

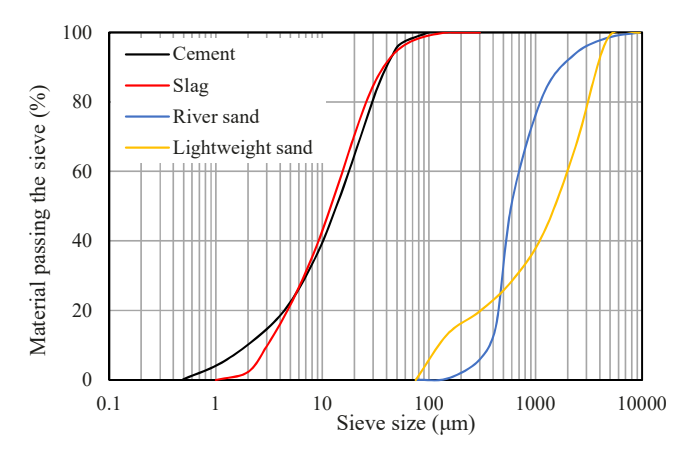


Fig. 3. The particle size distribution of raw materials.

with pre-saturated LWS or SRA. The proper content of LWS and SRA in UHPC were referred to previous research [1,48].

#### 3. Experimental methods

#### 3.1. Mixing and specimen preparation

The Hobart® HL-200 mixer [49], which has a volume capacity of 12 liters, was utilized to prepare UHPC mixtures. Detailed mixing procedures established from prior research was employed for the control mixtures (i.e., Reference, EA2, EA4, EA6, EA4S2, and EA4L25), including four steps: (1) dry ingredients, including cement, slag, CaO-type EA, RS, and LWS, were added and mixed at a speed of 107 RPM for a duration of 2 minutes. (2) the HRWR admixture and shrinkage-reducing agent (SRA) were dissolved in the mixing water to form the solution. And 90% of the dissolved solution was added and mixed at a speed of 107 RPM for 3 minutes. (3) the remaining portion of the solution was added and mixed at a speed of 198 RPM for 3 minutes. (4) steel fibers were incorporated and mixed at a speed of 198 RPM for 2 minutes. For other mixtures, the EA is added into the mixing water and continuously prewet through magnetic stirrer for 15 min, 30 min, or 45 min before the mixing process.

Homogenized fresh UHPC was utilized to produce cubic specimens, cylinder specimens, and prism specimens. During the casting process, the cast samples were put on a vibration table to ensure a high-quality casting. Right after the casting, the specimens were covered by damp burlap to maintain their moisture content. After 24 hours, the specimens were demolded and subsequently cured in lime-saturated water at room temperature (23  $\pm$  2 °C) until the testing.

#### 3.2. Fresh and hardened properties

The air content and mini slump flow values of UHPC were measured in according with ASTM C138 [50] and ASTM C230 [51]. All measurements were performed three times to calculate the average value.

The compressive strength of UHPC was conducted by uniaxial compressive tests on 50-mm cubes, following the guidelines specified in ASTM C109 [52]. The compression test setup is 250 K Gilson Compression Machine [53]. The splitting tensile strength was evaluated in according with ASTM C496 [54]. The test specimens were 76 mm  $\times$  152 mm cylinders. The splitting tensile test setup is Instron 5982 Universal Testing System [55]. A constant loading rate of 1.8 kN/min was maintained during the compressive testing process. The mechanical strengths of UHPC were conducted at 1, 3, 7, 14, and 28 days, respectively. All measurements were performed three times to calculate the average value. The splitting tensile strength (fspl) was calculated using Eq. (1):

**Table 2**Mixture proportions of UHPC (kg/m<sup>3</sup>).

Mixture	Cement	Slag	EA	RS	LWS	HRWR	SRA	Water	SF
Test group									
Reference	459.0	633.9	0	965.4	0	9.8	0	244.9	156.0
EA2	447.5	623.2	22.9	965.2	0	9.8	0	245.0	156.0
EA4	435.9	612.5	45.9	965.0	0	9.8	0	245.2	156.0
EA6	424.3	601.8	68.8	964.8	0	9.8	0	254.4	156.0
EA4-P15	435.9	612.5	45.9	965.0	0	9.8	0	245.2	156.0
EA4-P30	435.9	612.5	45.9	965.0	0	9.8	0	245.2	156.0
EA4-P45	435.9	612.5	45.9	965.0	0	9.8	0	245.2	156.0
Validation group									
EA4L50	435.9	612.5	45.9	482.7	327.9	6.0	0	247.8	156.0
EA4L50-P45	435.9	612.5	45.9	482.7	327.9	6.0	0	247.8	156.0
EA4S2	435.9	612.5	45.9	965.0	0	9.8	22.0	223.2	156.0
EA4S2-P45	435.9	612.5	45.9	965.0	0	9.8	22.0	223.2	156.0

Note: EA represents CaO-type expansive agent; RS represents river sand; LWS represents lightweight sand; HRWR represents high-range water reducer; SRA represents shrinkage-reducing agent; SF represents steel fiber.

$$f_{spl} = \frac{2 \times F}{\pi \times L \times D} \tag{1}$$

where  $f_{spl}$  represents the splitting tensile strength, in MPa; F represents peak load, in N; L represents sample length, in mm; and D represents sample diameters, in mm, respectively.

To analyze the cracking potentials of UHPC, it is necessary to propose an equation that predicts the development of tensile strengths with age. This equation will allow for estimation of the splitting tensile strength at various time points, considering the limited availability of the experimental data. The tensile strength development of UHPC exhibited close relationship with the hydration degree [56]. Therefore, the following equations (Eq. (2) and Eq. (3)) were adopted based on Janasson [57].

$$f_t = 0.77 \times f_{spl} + 0.21 \tag{2}$$

$$f_t(t) = f_{t,28} \times \exp\{-\lambda_1 \times [\ln(1 + (t - t_0))]^{-k_1}\}$$
(3)

where  $f_{spl}$  represents the splitting tensile strength, in MPa;  $f_t$  represents the axial tensile strength, in MPa;  $f_t(t)$  represents development of axial tensile strength with time, in MPa;  $f_{t,28}$  represents 28-d axial tensile strength, in MPa,  $t_0$  represents the time when the shrinkage stress first develops, and  $\lambda_1$ ,  $k_1$  represent the fitting parameters.

#### 3.3. Hydration heat

The hydration heat evolution of UHPC was assessed using an isothermal calorimeter (Model: Calmetrix® I-Cal 4000 HPC) [58]. The calorimeter was set to keep the sample at a constant temperature of 25 °C. Approximately 65 g of fresh UHPC was filled and sealed in a plastic cup and stored within the calorimeter. Starting from 2 minutes after the completion of mixing, the hydration heat evolution was continuously monitored for a duration of 48 hours.

#### 3.4. Shrinkage behaviors

The autogenous shrinkage of investigated UHPC was tested based on ASTM C1698 [59]. After mixing process, the fresh UHPC (with steel fibers) was cast as prism specimens measuring 25 mm  $\times$  25 mm  $\times$  280 mm and then sealed with water-proof alumina tap to prevent moisture loss. The length change of the specimens was measured by the test setup (Model: HM-250D) [60]. Subsequently, the prism samples were demolded and firstly recorded at the "time-zero" point which was determined in Section 4.3.1. Finally, the data was collected daily until 28 days. Three sample replicates were prepared for each test, and the average results for each test were reported.

The restrained shrinkage was evaluated in accordance with the JCI recommendations [61]. The prismatic specimen with dimension of  $100~\text{mm} \times 100~\text{mm}$  and length of 1000~mm was prepared. The purpose

of utilizing 19.1 mm nominal diameter deformed steel rebar was to control the volume change caused by shrinkage in UHPC. Table 3 provides comprehensive information regarding the properties of steel rebars

To ensure uniform shrinkage stress at the center of the steel rebar, the ribbed edges of the rebars were smoothed by lathing and then protected with a Teflon sheet. This precautionary measure effectively prevented any frictions between the UHPC and the rebar [61]. In addition, the 350-mm embedment length at both ends was set to ensure the enough shrinkage stress [56], as shown in Fig. 4(a). A fiber optic sensor system (as shown in Fig. 4(b)) was affixed to the center of the steel rebar. This sensor system was utilized to accurately measure both strain and temperature variations in real-time [62–64]. For the restrained shrinkage test, samples were demolded after 24 hours and sealed with aluminum adhesive tapes to prevent the moisture loss.

According to the ASTM C1698 [59] and JCI recommendations [61], the first shrinkage measurement is performed at initial setting time to eliminate the influence of volume changes that occur while the concrete is still in its fresh state. However, previous studies found both the initial and final setting time are inappropriate as the zero point for autogenous shrinkage measurement because the significant shrinkage strain in very-early ages was ignored [65]. In order to more accurately evaluate the cracking potentials of UHPC mixtures in this research, the zero point of autogenous shrinkage measurement, called "time-zero", is defined as the moment when shrinkage stress begins in UHPC [56,66], which is determined in Section 4.3.

#### 3.5. Thermogravimetry analysis

A thermal analyzer (Model: TA® TG55) [29] was utilized to conduct thermogravimetric analysis. For the sample preparation, dried slices were taken, and 50 mg of the samples were finely powdered after halting hydration with isopropanol. The powder was subjected to vacuum drying for 24 hours prior to experiments. Then, the sample was heated steadily from 20 °C to 600 °C at a constant rate of 20 °C/min in a nitrogen flow. Each curve shows two major peaks corresponding to: (1) the dehydration of C-S-H, ettringite, and AFm phases, up to 400 °C and (2) the dihydroxylation of Portlandite from 400 °C to 500 °C [29].

**Table 3**Properties of restrained steel rebar.

Code	d <sub>r</sub> (mm)	A <sub>r</sub> (mm <sup>2</sup> )	E <sub>r</sub> (GPa)	f <sub>y</sub> (MPa)	$\epsilon_{y}$ (mm/mm)	f <sub>u</sub> (MPa)
#6 Steel Rebar	19.1	286.5	200.0	508.5	0.00254	625.2

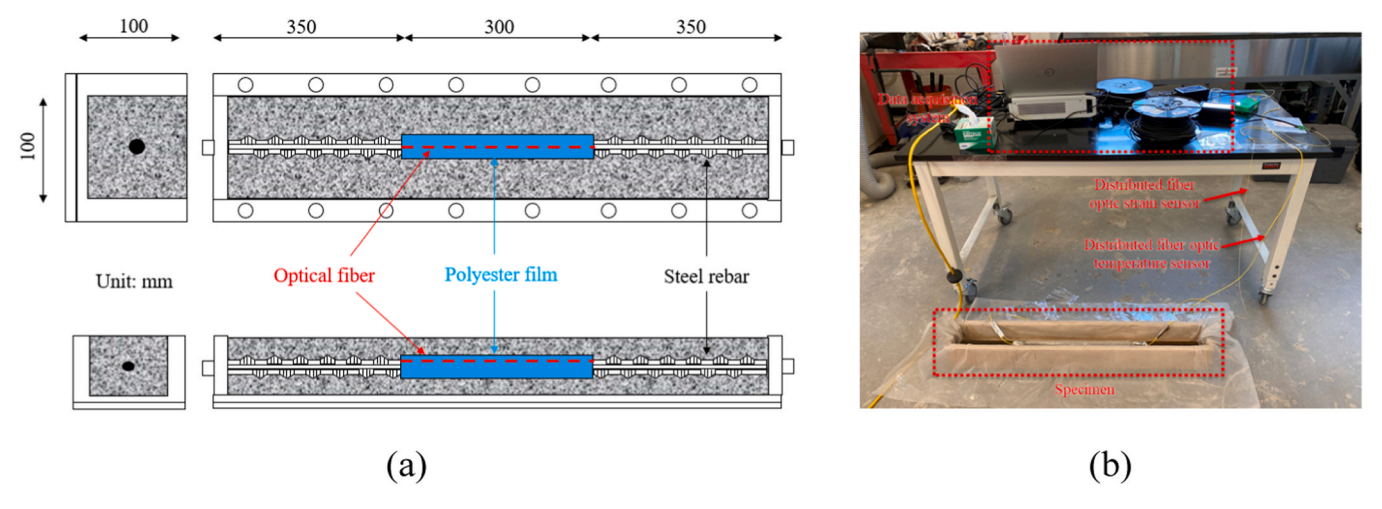


Fig. 4. Test setup for restrained autogenous shrinkage measurement: (a) the schematic diagram of the device; (b) the image of test device.

### 3.6. Scanning electron microscopy with energy dispersive X-ray spectroscopy

The scanning electron microscopy with energy dispersive X-ray spectroscopy (SEM-EDX, Model: LMSI Apreo 2 SEM) was utilized to track the evolution of the EA during the prewetting process [67]. The original EA powder was directly subjected to vacuum drying for 24 hours prior to experiments. Besides, the prewet EA powder was added into the water and continuously mixed through magnetic stirrer for 45 min. Afterwards, the prewet EA powder was subjected to vacuum drying for 24 hours prior to experiments. The microstructure of original and prewet EA powder were inspected using the ETD detector at 8 kV voltage.

#### 4. Experimental results

#### 4.1. Fresh properties

Fresh properties of cement-based materials are closely related to construction quality. Poor workability and high air contents result in difficult placement and poor compaction [68–70]. Fig. 5 plots the mini slump flow and air contents of UHPC mixtures. The columns represent the average results, while the error bars indicate the standard deviations.

As the EA contents increased from 0% to 6%, the mini-slump spreads of UHPC were reduced from 280 mm to 240 mm by 15% and the air

contents were increased from 3.2% to 4.5%. The results indicated that the addition of EA reduced the flowability and increased the air contents in fresh UHPC which exhibit strong agreement with the findings from Li et al. [71] and Pan et al. [72]. It is attributed to the high specific surface area and high reactivity of EA which consumes free water for the lubrication to undermine the fresh properties [71,72]. In comparison, as the prewet time increased to 45 min, the mini-slump spreads were reduced by 4.0%, 3.5%, and 4.2% for EA4, EA4L50, and EA4S2, respectively. Besides, the air contents slightly ranged from 3% to 5%, which indicates the prewet process has a slight effect on the fresh properties, which is promising for the UHPC production on job sites.

#### 4.2. Mechanical properties

#### 4.2.1. Compressive strength

Fig. 6 plots compressive strength results of investigated UHPC mixtures. The columns depict the average results, while the error bars indicate the standard deviations. Fig. 6(a) shows that, as the EA contents increased from 0% to 4%, the compressive strengths at 1 day, 3 days, 7 days, and 28 days were increased by 14%, 8%, 4%, and 3%, respectively. However, as the EA contents further increased from 4% to 6%, the compressive strengths at 1 day, 3 days, 7 days, and 28 days were decreased by 12.4%, 8.2%, 5.9%, and 7.1%, respectively. Results clearly indicated that the proper addition of EA efficiently improves the earlyage compressive strengths of UHPC, especially at the early ages ( $\leq$  3 days), while the excessive EA additions (i.e.,  $\geq$  6% in this research)

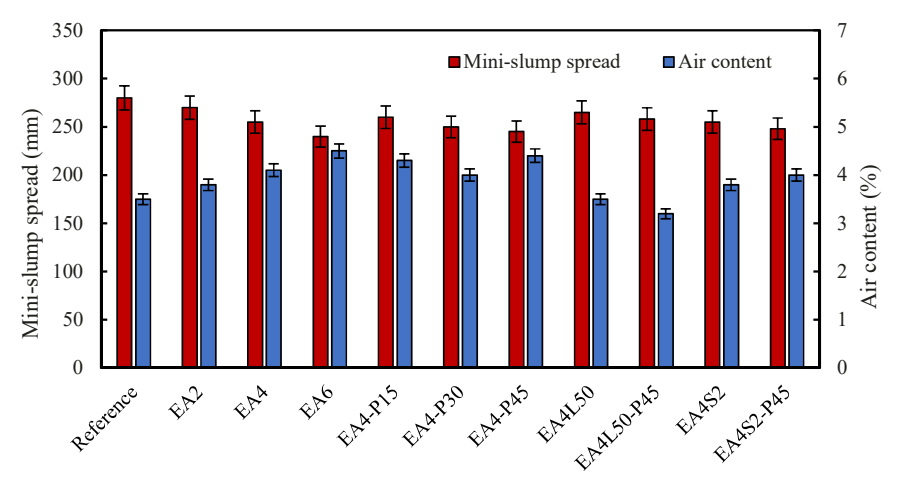


Fig. 5. Results of mini-slump spreads and air contents of investigated UHPC mixtures.

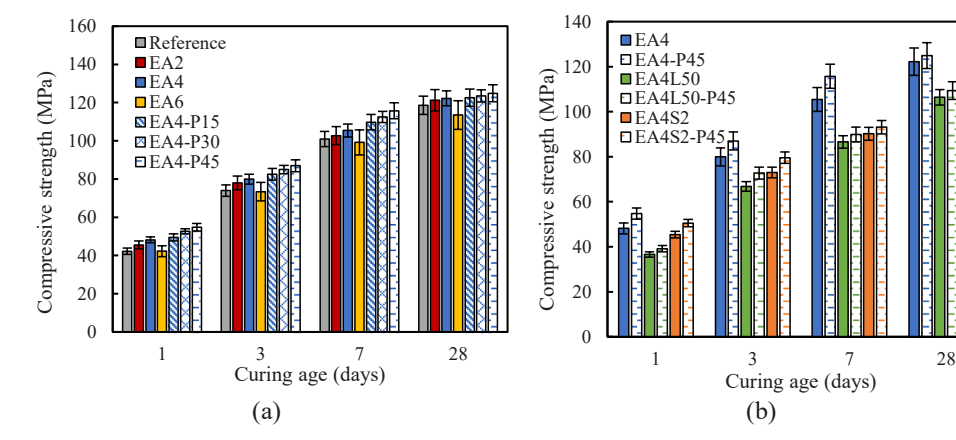


Fig. 6. Results of compressive strengths of all investigated UHPC mixtures.

decreases the compressive strength of UHPC. The negative effect on compressive strength is attributed to the possible microcracks resulting from the excessive expansion products (i.e., portlandite) and reduced hydration products due to the replacement of cementitious materials [73,74]. This explanation is supported by previous studies [36].

Fig. 6(b) shows the effect of prewet time on compressive strengths for EA4, EA4L50, and EA4S2, respectively. As the prewet time increased to 45 min, the compressive strengths of EA4 at 1 day, 3 days, 7 days, and 28 days were increased by 13.7%, 8.7%, 9.2%, and 2%. Besides, the compressive strengths of EA4L50 at 1 day, 3 days, 7 days, and 28 days were increases by 8.2%, 8.8%, 5.1%, and 3.5%. In addition, the compressive strengths of EAS2 were increased by 11.2%, 8.9%, 3.3%, 3.2%. Results indicated that prewetting the EA with the mixing water can improve the compressive strengths, especially at early ages ( $\leq$  3 days). It was speculated that the prewet EA with the mixing water accelerated the hydraulic reaction and increased the expansion products, which were validated in Section 5.1 and Section 5.2.

#### 4.2.2. Splitting tensile strength

Fig. 7 plots splitting tensile strength results of investigated UHPC mixtures. The columns depict the average results, while the error bars indicate the standard deviations. Fig. 7(a) shows that, as the EA contents increased from 0% to 4%, the splitting tensile strengths at 1 day, 3 days, 7 days, and 28 days were increased by 26.9%, 22.3%, 19.6%, and 6.5%. However, as the EA contents further increased from 4% to 6%, the splitting tensile strengths at 1 day, 3 days, 7 days, and 28 days were decreased by 4.4%, 14.0%, 8.5%, and 7.4%. Fig. 7(b) shows the effect of prewet time on splitting tensile strengths for EA4, EA4L50, and EA4S2, respectively. As the prewet time increased to 45 min, the splitting tensile strengths of EA4 at 1 day, 3 days, 7 days, and 28 days were increased by 13.7%, 7.9%, 6.5%, and 5.3%. Besides, the splitting tensile strengths of

EA4L50 at 1 day, 3 days, 7 days, and 28 days were increased by 11.1%, 10.4%, 3.7%, and 2.5%. In addition, the splitting tensile strengths of EAS2 were increased by 13.3%, 8.9%, 4.4%, and 3.3%. Similarly, results showed the proper EA contents and prewet EA with the mixing water improved the splitting tensile strengths, especially at early ages ( $\leq$  3 days). The mechanisms were elaborated in Section 4.2.1.

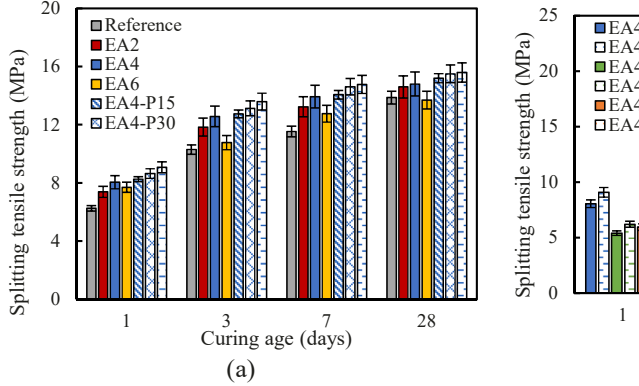
Although the tensile properties of investigated UHPC are only measured at 1, 3, 7, 14, and 28 days, Yoo et al. [75] reported that the tensile strength of UHPC showed the S-shaped development curve that was similar with the hydration curve. Therefore, in according with previous research [66,76], the Eq. (2) and Eq. (3) are cited to fit the development of tensile strengths and then show the continuous development of tensile properties with curing age. Table 4 summarized the tested splitting tensile strengths, calculated axial tensile strengths, and regression coefficients of the predicting models. As shown in Fig. A1 in Appendix and Table 4, all coefficients of R<sup>2</sup> are higher than 0.95, representing the strong agreement with experimental results.

#### 4.3. Autogenous shrinkage behaviors

#### 4.3.1. "Time-zero" determination of shrinkage measurement

The "time-zero" determination is the basic to measure the precise shrinkage strain, thus evaluating the cracking potentials of UHPC mixtures. Previous studies indicated that the start time of shrinkage stress in the steel rebar should be defined as the "time-zero" of the restrained shrinkage measurement [66]. In this study, the optical fiber system (shown in Fig. 8) was applied to measure the deformation and stress of steel rebar caused by the shrinkage stress and determine the "time-zero" of different UHPC mixtures.

Taking three UHPC mixtures (e.g., EA4, EA4L50, and EA4S2) as the example shown in Fig. 8(a), the reinforced rebars showed limited



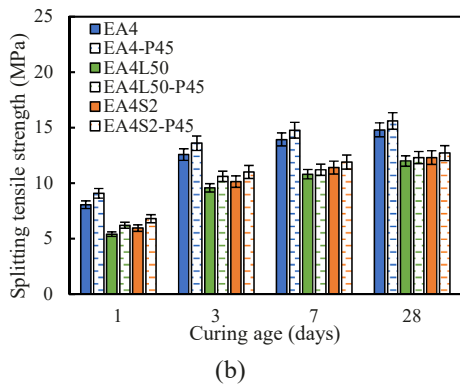


Fig. 7. Results of splitting tensile strengths of investigated UHPC mixtures.

**Table 4**Summarized tensile strengths and regression coefficients.

Mixture design	Splitting tensile strength (MPa)			Axial tensile strength (MPa)				$\lambda_1$	$k_1$	R <sup>2</sup>	
	1 d	3 d	7 d	28 d	1 d	3 d	7 d	28 d			
Reference	6.3	10.3	11.5	13.9	5.1	8.1	9.1	10.9	0.3707	1.2896	0.95
EA2	7.4	11.8	13.2	14.6	5.9	9.3	10.4	11.5	0.2823	1.5099	0.98
EA4	8.0	12.6	13.9	14.8	6.4	9.9	10.9	11.6	0.2239	1.6982	0.99
EA6	7.7	10.8	12.8	13.7	6.1	8.5	10.1	10.8	0.2602	1.4095	0.95
EA4-P15	8.3	12.7	14.1	15.2	6.6	10	11.1	11.9	0.2346	1.6081	0.99
EA4-P30	8.6	13.1	14.6	15.5	6.8	10.3	11.5	12.1	0.2170	1.7019	0.99
EA4-P45	9.1	13.6	14.8	15.6	7.2	10.7	11.6	12.2	0.1911	1.7598	0.99
EA4L50	5.4	9.6	10.8	12.0	4.4	7.6	8.5	9.5	0.3125	1.5761	0.98
EA4L50-P45	6.0	10.2	11.1	12.4	4.8	8.1	8.8	9.8	0.2833	1.6059	0.99
EA4S2	6.0	10.1	11.4	12.3	4.8	8	9	9.7	0.2680	1.6826	0.99
EA4S2-P45	6.6	10.7	11.8	12.6	5.3	8.4	9.3	9.9	0.2326	1.7180	0.99

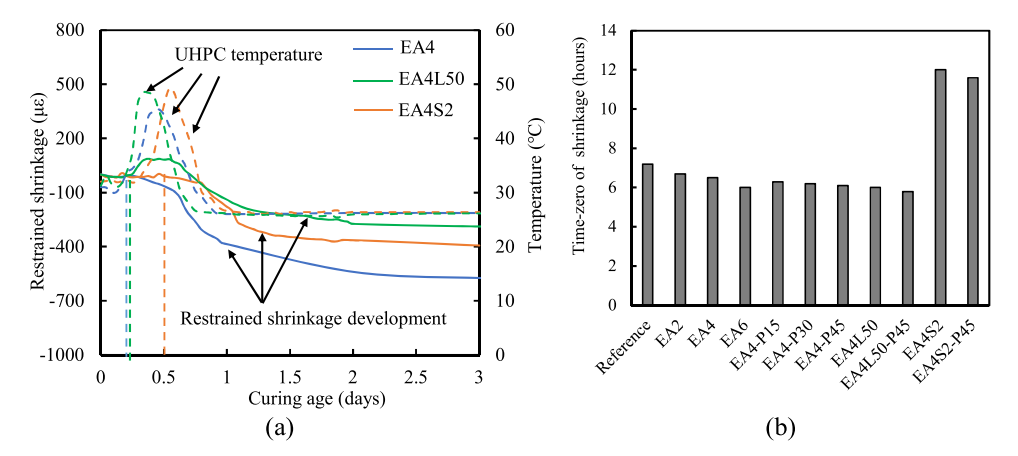


Fig. 8. The "time-zero" measurement of autogenous shrinkage of all investigated UHPC mixtures: (a) early-age shrinkage strain and temperature variation in reinforced rebars: (b) summarized results of "time-zero" of investigated UHPC mixtures.

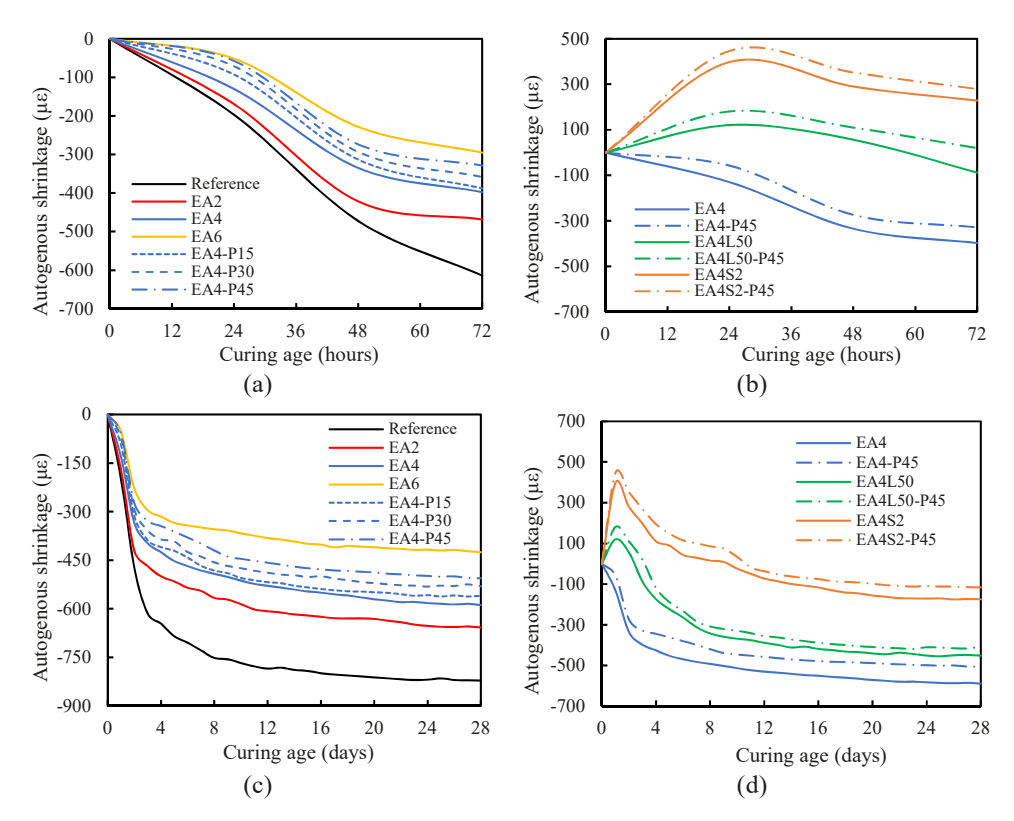


Fig. 9. Results of autogenous shrinkage of investigated UHPC mixtures: (a-b) early-age (≤ 3 days) autogenous shrinkage; (c-d) autogenous shrinkage up to 28 days.

deformation at the beginning due to the nearly zero stiffness of investigated UHPC mixtures at the fresh status. Subsequently, the reinforced rebars started to deform due to the generated shrinkage stress and the increased stiffness in the UHPC. The start time of the restrained shrinkage development was regarded as the "time-zero". Results indicated the "time-zero" is varied for three different UHPC mixtures, which are 0.27 days (6.5 hours), 0.25 days (6.0 hours), and 0.5 days (12 hours) for EA4, EA4L50, and EA4S2 because the addition of lightweight sand and/or shrinkage-reducing agent affects the hydration of UHPC matrix, which was validated in Section 5.1. Based on this, the "time-zero" of remaining UHPC mixtures in this research were determined and summarized in Fig. 8(b).

#### 4.3.2. Results of autogenous shrinkage

Fig. 9 plots autogenous shrinkage results (up to 28 days) of investigated UHPC mixtures. The presented results are the average values of three parallel specimens. Fig. 9(a) and Fig. 9(c) show that, as the EA contents increased from 0% to 6%, 3-day autogenous shrinkage was decreased from 614  $\mu\epsilon$  to 295  $\mu\epsilon$  (by 52%) and 28-day autogenous shrinkage was decreased from 822  $\mu\epsilon$  to 425  $\mu\epsilon$  (by 45%). It indicated that the addition of expansive agent dramatically reduces autogenous shrinkage of investigated UHPC mixtures, particularly during the early ages. The underlying mechanism is that the CaO-type expansive agents can react with the mixing water to generate the expansive product (i.e., Portlandite) during the hardening of UHPC which compensates for the shrinkage stress to reduce the autogenous shrinkage [2].

Fig. 9(b) and Fig. 9(d) show that, as the prewet time increased from 0 min to 45 min, the 3-day autogenous shrinkage of EA4 was further decreased from 397  $\,\mu \epsilon$  to 328  $\,\mu \epsilon$  (by 17%); the 3-day autogenous shrinkage of EA4L50 was eliminated and the 3-day expansion was 19  $\,\mu \epsilon$ ; the 3-day expansion of EA4S2 was increased from 218  $\,\mu \epsilon$  to 279  $\,\mu \epsilon$  (by 28%). In addition, the 28-day autogenous shrinkage of EA4, EA4L50, and EA4S2 were decreased from 589  $\,\mu \epsilon$  to 472  $\,\mu \epsilon$  (by 20%), from 452  $\,\mu \epsilon$  to 402  $\,\mu \epsilon$  (by 12%), and from 174  $\,\mu \epsilon$  to 114  $\,\mu \epsilon$  (by 34%), respectively. Results indicated the prewet expansive agent with water improves the expansion effect and further reduces the autogenous shrinkage of investigated UHPC mixtures. It was speculated that prewet expansive agent with the mixing water increased the expansive products, which was validated in Section 5.2.

#### 4.4. Restrained shrinkage behaviors and cracking potential evaluation

Due to the significant shrinkage reduction effect, previous studies were in good agreement that the proper addition of expansive agent reduced the cracking potentials of cementitious materials [26]. In comparison, the effect of the new method proposed in this study, i.e., prewet expansive agent before the UHPC mixing process, on both the early-age strength and autogenous shrinkage are relatively limited. Its effect on the cracking potentials of UHPC mixtures is still unknown. Therefore, the effect of prewet expansive agent on cracking potentials of UHPC was quantified and validated.

In the Appendix, **Fig. A2** plots the measured and restrained shrinkage results (up to 28 days) of EA4, EA4L50, and EA4S2 in the validation group. The presented results are the average values of two parallel specimens. The UHPC specimen size of restrained shrinkage tests (i.e.,  $100 \times 100 \times 1000 \text{ mm}^3$ ) is large, and the hydration heat generated by the UHPC specimens cannot be ignored. Thus, the thermal dilation strains of the reinforced rebar need to be subtracted from the measured strain according to Eq. (4) to get the precise restrained shrinkage. A constant coefficient of thermal expansion (CTE) of  $11 \, \mu\text{e/°C}$  was used in this study [59].

$$\varepsilon_{as} = \varepsilon_m - \alpha_T \times \Delta T \tag{4}$$

where  $\varepsilon_{as}$  represents the real restrained shrinkage;  $\varepsilon_m$  represents the measured autogenous shrinkage;  $\alpha_T$  represents the CTE of UHPC;  $\Delta T$ 

represents the temperature variance during curing process, in °C.

Fig. 10 summarizes the restrained shrinkage results without the temperature dilation effect. As the prewet time increased to 45 min, the 28-day restrained shrinkage were reduced from 644  $\mu\epsilon$  to 586  $\mu\epsilon$  (by 10%), from 449  $\mu\epsilon$  to 366  $\mu\epsilon$  (by 18%), from 345  $\mu\epsilon$  to 293  $\mu\epsilon$  (by 15%) for EA4, EA4L50, and EA4S2, respectively. Results clearly showed that, apart from the autogenous shrinkage, the premixing expansive agent with water further reduced the restrained shrinkage of investigated UHPC as well. Subsequently, the restrained shrinkage stress should be determined based on the restrained shrinkage strain. The JCI committee proposed the Eq. (5) to calculate the autogenous shrinkage stress in UHPC using the following method:

$$\sigma_c = \frac{E_r \times \varepsilon_r \times A_r}{A_c} \tag{5}$$

where  $E_r$  represents the elastic modulus of rebar, in GPa;  $\varepsilon_r$  represents the strain obtained in rebar without the thermal dilation, in  $\mu\varepsilon$ ; and  $A_r$  and  $A_c$  are the areas of the rebar and concrete, in mm<sup>2</sup>.

Fig. 11 plots the calculated restrained shrinkage stress development and the calculated axial tensile strength development with curing ages of investigated UHPC mixtures. In general, for all investigated UHPC mixtures, the axial tensile strength significantly surpassed the autogenous shrinkage stress. Therefore, the limited cracking potential exists until 28 days. Moreover, it was apparent that, compared to the control UHPC mixtures (e.g., EA4, EA4L50, EA4S2), the UHPC mixtures with prewet EA (e.g., EA4-P45, EA4L50-P45, and EA4S2-P45) exhibited the higher axial tensile strength and the lower restrained shrinkage stress. Results showed that the prewet expansive agent with mixing water is a promising method to further reduce the cracking potentials of UHPC mixtures. The cracking potentials were calculated by dividing the restrained shrinkage stress ( $\sigma_c$ ) by the axial tensile strength ( $f_t$ ) which is expressed as Eq. (6), which was cited from the previous research [56]:

$$\Theta_{qp}(t) = \frac{\sigma_c(t)}{f_t(t)} \tag{6}$$

where  $\Theta_{cp}(t)$  represents the cracking potential with curing age;  $\sigma_c(t)$  represents the restrained shrinkage stress, in MPa; and  $f_t(t)$  represents the axial tensile strength; in MPa.

Fig. 12(a) and Fig. 12(b) show the cracking potentials of investigated UHPC mixtures, and all cracking potentials of investigated UHPC mixtures were below 1. However, the shrinkage stress from the restrained prismatic test is not totally the same with the axial tensile stress from the experimental test, thus the cracking potentials below 1 does not represent the investigated UHPC mixtures will not crack during the applications. In addition, it is apparent noting that compared to the EA4, EA4L50, and EA4S2, the EA4-P45, EA4L50-P45, and EA4S2-P45 exhibited much lower cracking potentials until 28 days. In order to accurately quantify the cracking potentials, two new parameters are proposed in this research for the first time: (1) peak cracking potential represents the maximum ratio of restrained shrinkage stress to the tensile strength, indicating the highest possibility of shrinkage-induced cracking; (2) cumulative cracking potential represents the cumulative ratio of restrained shrinkage stress to the tensile strength up to 28 days, indicating the cumulative possibility of shrinkage-induced cracking. Results show that the peaking cracking potential and cumulative cracking potential were reduced by 18% and 14% (by comparing EA4 and EA4-P45), 32% and 25% (by comparing EA4L50 and EA4L50-P45), and 8% and 18% (by comparing EA4S2 and EA4S2-P45), show in Fig. 12 (c). It validated the prewet expansive agent with mixing water is a promising method to reduce the cracking potentials.

#### 5. Discussions

Based on the aforementioned experimental results, it is evident that the investigated low-shrinkage UHPC mixtures (e.g., mono EA addition,

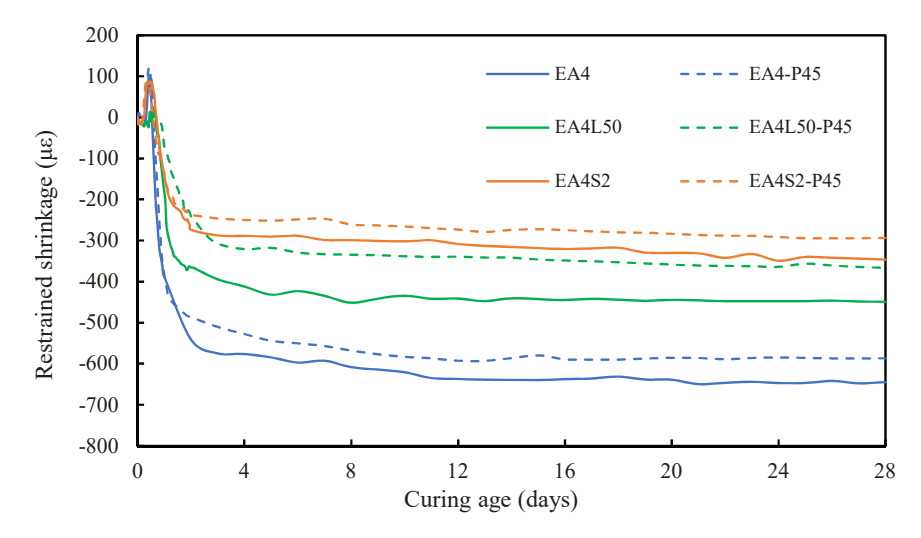


Fig. 10. Summarized restrained shrinkage without temperature dilation effect. Note: the restrained shrinkage is the measured shrinkage minus the temperature effect.

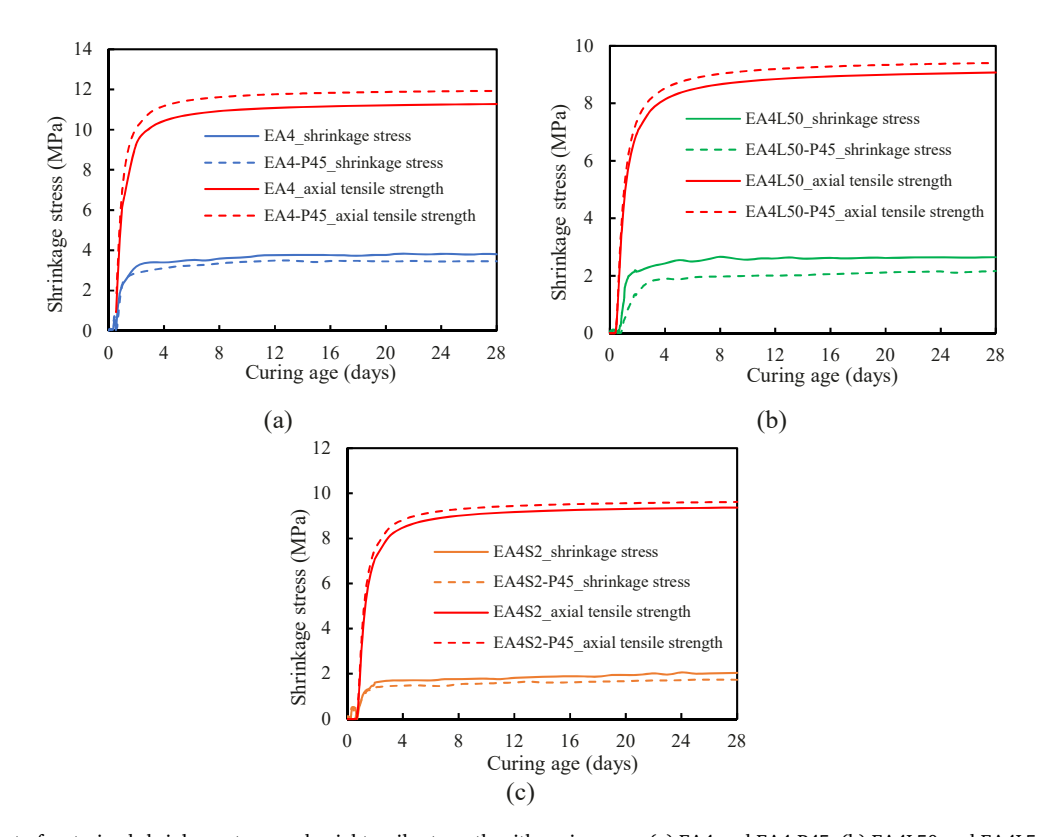


Fig. 11. Development of restrained shrinkage stress and axial tensile strength with curing ages: (a) EA4 and EA4-P45; (b) EA4L50 and EA4L50-P45; and (c) EA4S2 and EA4S2-P45.

combined EA and lightweight sand (LWS) addition, and combined EA and shrinkage-reducing agent (SRA) addition) behaved quite differently in the cracking potentials.

Fig. 13 compares the mechanisms with and without EA premix for the UHPC mixtures with mono EA addition. Due to the low permeability, lack of free water, and low EA addition (e.g., < 5% by volume of binders in UHPC) in the UHPC matrix, only a small amount of EA particles can react with free water to generate the expansion products, leading to the rest portion of EA particles merely being expensive fillers. Therefore, the direct addition of EA in UHPC (i.e., the traditional method) showed relatively limited mitigation on the cracking potentials of UHPC [36]. On the contrary, for the prewet EA, the EA particles sufficiently

contacted with free water and absorbed more water for expansion reaction (this is validated in Section 5.2). The extra expanded volume fills more pores in UHPC for the shrinkage mitigation [71]. Compared with the UHPC without prewet EA, the peak and cumulative cracking potentials of UHPC with prewet were reduced by 18% and 14%, respectively. In addition, more EA reaction products (i.e., portlandite) were generated by the prewet EA method, which is beneficial for the strength development of UHPC, as evidenced in Sections 4.2 and 5.1. The EA prewet method accelerated the hydration heat evolution and increased the mechanical strength, especially at early ages.

Fig. 14 shows the underlying mechanism for investigated UHPC mixtures with combined EA and LWS addition. Compared to the mono

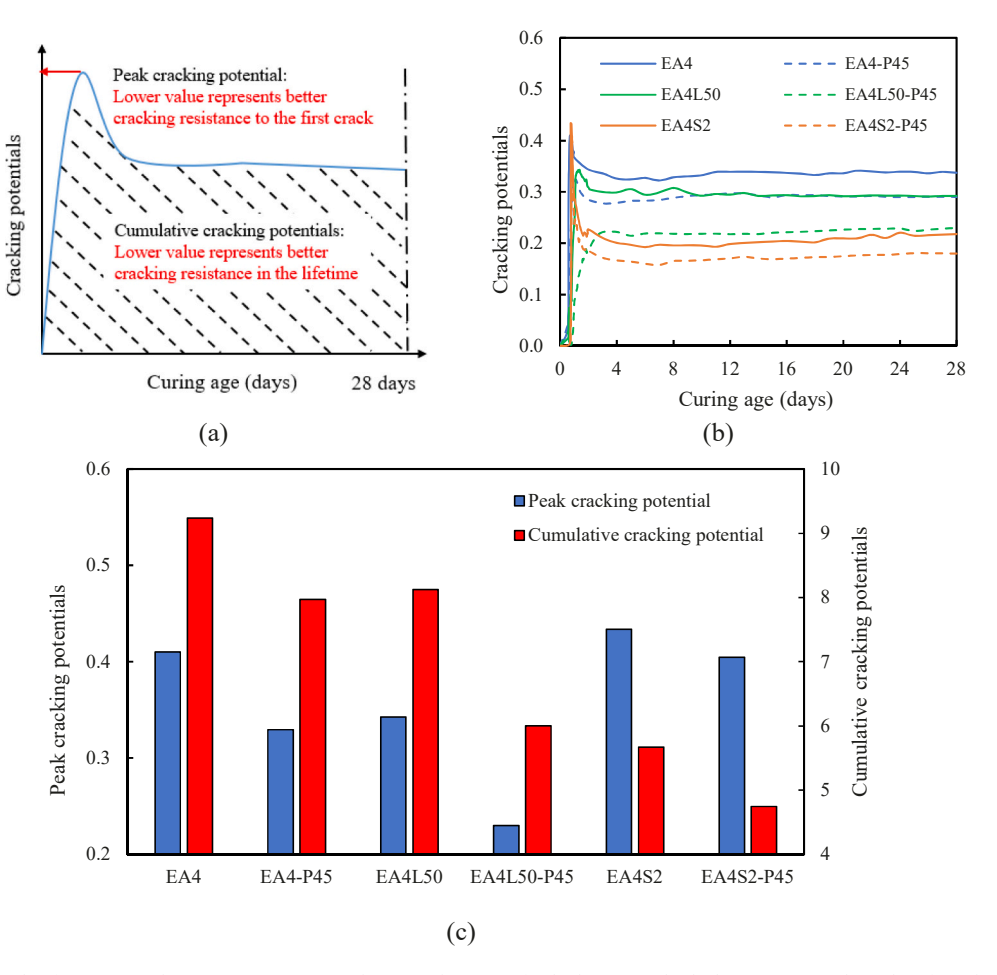


Fig. 12. Cracking potentials of investigated UHPC mixtures: (a) schematic diagram of calculation method; (b) experimental results of cracking potentials of UHPC mixtures; (c) summarized peak cracking potentials and cumulative cracking potentials.

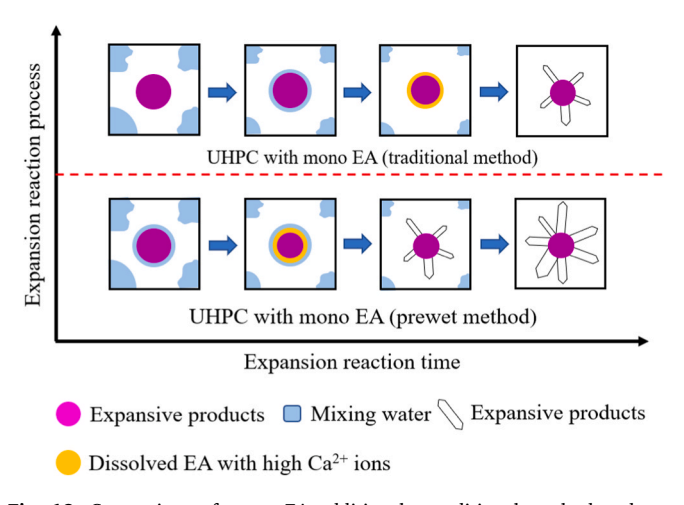


Fig. 13. Comparison of mono EA addition by traditional method and prewet method.

EA addition, the combined use of pre-saturated LWS and EA shows more pronounced effect to reduce the cracking potentials of UHPC because: (1) the pre-saturated LWS can gradually release the absorbed water to the adjacent UHPC matrix to mitigate the self-desiccation effect [35]; (2) the released free water can contact the unreacted EA to form more expansive products [39], shown in Section 5.2. Moreover, the formation of expansive products is not only restrained by the limited free water but also restrained by the limited space in the dense UHPC matrix [36].

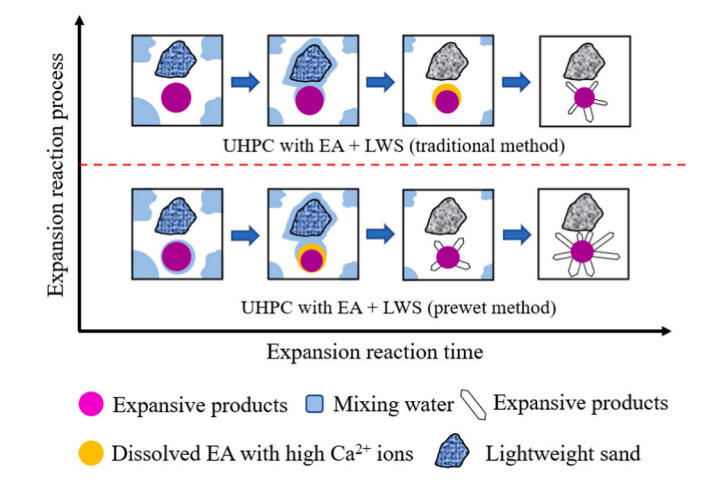


Fig. 14. Comparison of combined EA and LWS addition in UHPC by traditional method and prewet method.

Given that the porous structure of LWS can provide more spaces for EA reaction after fully releasing the absorbed water, thus the effect of EA prewet method was further enhanced when the LWS was involved. Specifically, by applying the prewet EA method, the peak and cumulative cracking potentials of UHPC with combined EA and LWS addition were further reduced by 32% and 25%, respectively. Similarly, for UHPC mixtures with combined EA and LWS addition, the EA prewet method accelerated the hydration heat evolution shown in Section 5.1,

increased the portlandite contents shown in Section 5.2, and enhanced the mechanical strength, particularly at early ages shown in Section 4.2.

Fig. 15 shows the underlying mechanism for investigated UHPC mixtures with combined EA and SRA addition. Compared to the mono EA addition, the combined use of SRA and EA shows more dramatic effect to reduce the cracking potentials of UHPC as well, because (1) SRA particles have the ability to adhere to the water-solid interface, and the electrostatic repulsive force between these particles counteracts the shrinkage force. [2]; (2) the SRA particles can cover on cement particles surface to retard the cement hydration [39]. In this case, more free water and space can be saved for the generation of expansive products, thus the effect of EA prewet method was also further enhanced when the SRA was involved [73]. Specifically, by applying the prewet EA method, the peak and cumulative cracking potentials of UHPC with combined EA and LWS addition were further reduced by 8% and 18%, respectively. Similarly, for UHPC mixtures with combined EA and SRA addition, the prewet EA method accelerated the hydration heat evolution shown in Section 5.1, increased the portlandite contents shown in Section 5.2, and increased the mechanical strength of UHPC, especially at early ages shown in Section 4.2.

#### 5.1. Hydration heat

Fig. 16 shows the isothermal calorimetry results of investigated UHPC. Fig. 16(a) shows that, as the EA contents increased from 0% to 6%, the peak point of hydration heat flow was accelerated from 13.4 hours to 10.8 hours (by 20%), indicating that the addition of expansive agent promotes the hydraulic reaction. Besides, Fig. 16(b) shows that, as the prewet time of expansive agent increased to 45 min, the peak point of hydration heat flow was accelerated from 11.2 hours to 9.5 hours (by 12.5%), from 8.9 hours to 8.7 hours (by 3%), and from 17.8 hours to 15.6 hours (by 12.3%) for EA4, EA4L50, and EA4S2, respectively. Results also elaborated that the prewet expansive agent with mixing water is effective to promote the hydraulic reaction. These results validated the improved mechanical strengths of UHPC mixtures.

#### 5.2. Thermogravimetry analysis

Fig. 17 shows the thermogravimetry results of UHPC mixtures at 3 days. The rate of mass loss is indicated by derivative thermogravimetry (DTG), which represents the derivative of mass loss with respect to temperature change. Every DTG curve exhibited three prominent peaks that corresponded to the following processes: (1) dehydration of C-S-H, ettringite, and AFm phases, up to 400 °C; (2) dehydroxylation of CH, occurring between 400 °C and 500 °C; and (3) decarbonation of calcium

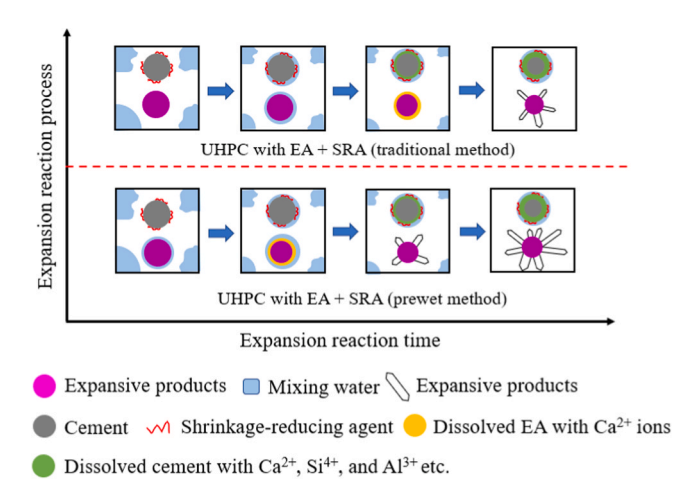


Fig. 15. Comparison of combined EA and SRA addition in UHPC by traditional method and prewet method.

carbonate, observed from 500 °C to 800 °C [29,77].

As the prewet time increased to 45 min, the CH contents normalized per 100 g mortar were increased by 15%, 8%, and 6% for EA4, EA4L50, and EA4S2, respectively. The results indicated that more CH contents were generated at 3 days by prewet expansive agent with the mixing water. Such results are in good agreement with results of hydration heat, mechanical properties (e.g., compressive strength and splitting tensile strength), and shrinkage behaviors.

#### 5.3. SEM-EDX observations

The SEM images of the original and prewet EA powder were shown in Fig. 18. For the original EA powder, the surfaces of the unhydrated EA particles were bare, shown in Fig. 18(a). By contrast, after 45 min of prewet process, some hexagonal-prism structures were found on the surface of prewet EA particles, shown in Fig. 18(b). According to the principles of the expansion reaction and the TGA results in Section 5.2, the hexagonal-prism structures should be calcium hydroxide [44]. In summary, the SEM-EDX observation showed the prewet EA method did promote the expansion reaction of the CaO-based EA, thus reducing the cracking potentials of UHPC mixtures.

#### 6. Conclusions

This research provides a viable method to promote the expansion reaction of EA in UHPC, thus reducing the cracking potential of UHPC. Specifically, the dry CaO-type EA powder was prewet with the mixing water prior to the mixing process to shorten the dormant period of expansive expansion. Comprehensive experiments were conducted to evaluate the effects of prewet time on fresh properties, mechanical strengths, and autogenous shrinkage. The restrained shrinkage tests were conducted to verify the reduction of cracking potentials of investigated UHPC. The underlying mechanisms of the effect of prewet Caotype EA in different UHPC were elaborated. The following conclusion are drawn:

- (1) Direct EA addition significantly affected fresh properties while EA prewet time had negligible effect. As EA contents increased to 6%, the mini slump was reduced by over 15% and the air contents increased over 30%. However, as the prewet time increased to 45 min, the reduction of mini-slump spreads and the increase of air contents were below 4% and 10%.
- (2) Proper EA addition and EA prewet method efficiently improved mechanical performance of UHPC. As the EA contents increased to 4%, the compressive strengths at 3 days and 28 days reached the peak values (i.e., 79.9 MPa and 122.2 MPa). Besides. as the prewet time increased to 45 min, the 3-day and 28-day compressive strengths were increased by 8.7% and 2% (EA4), 8.8% and 3.5% (EA4L50), and 8.9% and 3.2% (EA4S2). By contrast, EA prewet method showed pronounced effect in early ages.
- (3) Direct EA addition and EA prewet method reduced the autogenous shrinkage of UHPC. As EA contents increased to 6%, the 28-day cumulative autogenous shrinkage reduced by 45%. In comparison, as the prewet time increased to 45 min, the 28-day cumulative autogenous shrinkage of EA4, EA4L50, and EA4S2 decreased by 20%, by 12%, and by 34%, respectively. Obviously, directly increasing EA contents is more effective in inhibiting shrinkage of UHPC, compared to EA prewet method.
- (4) By further reducing shrinkage and increasing mechanical strength, EA prewet method was proven to be effective to further reduce the cracking potentials of UHPC at fixed EA contents. As the prewet time increased to 45 min, the peak and cumulative cracking potential were reduced by 18% and 14% (EA4), 32% and 25% (EA4L50), and 8% and 18% (EA4S2). By providing extra

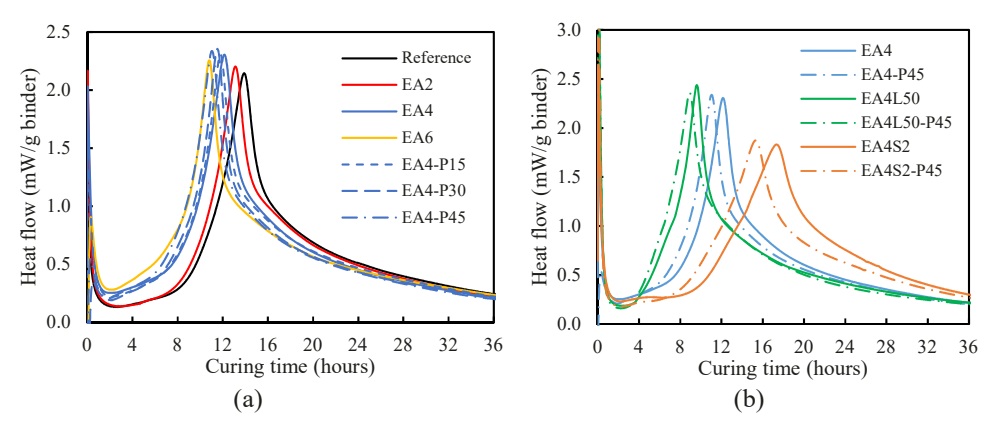


Fig. 16. Hydration heat results of (a) expansive agent content and (b) prewet time.

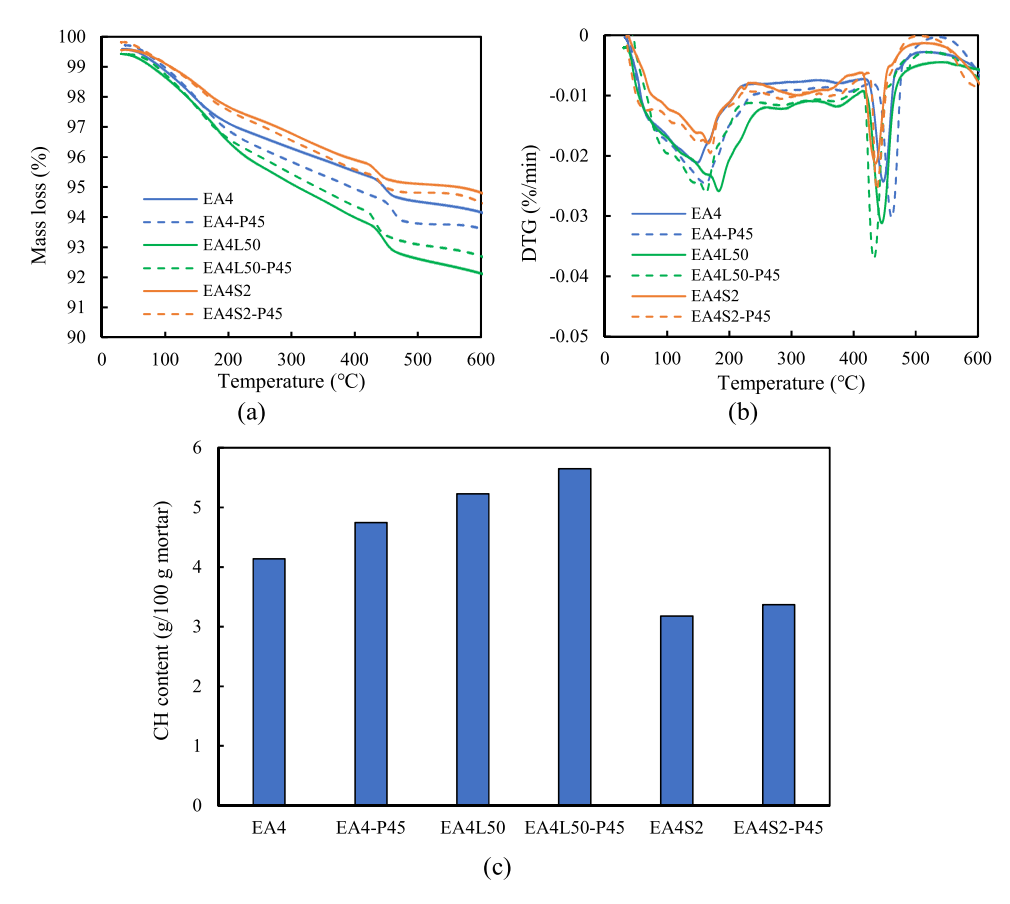


Fig. 17. Thermogravimetry results of investigated UHPC mixtures at 3 days.

free water and space, the combination of EA and LWS was the optimal strategy.

(5) The hydration heat and thermogravimetric analysis results showed that prewet dry CaO-type EA with mixing water prior to the mixing process accelerated the hydration process and increased the portlandite contents, which elaborated the underlying mechanisms of the effect of prewet CaO-type EA in different UHPC mixtures.

#### CRediT authorship contribution statement

**Xiao Tan:** Writing – review & editing, Validation, Investigation, Data curation. **Jiang Du:** Writing – original draft, Methodology, Investigation, Data curation, Conceptualization. **Weina Meng:** Writing –

review & editing, Supervision, Resources, Project administration, Methodology, Investigation, Funding acquisition. Yi Bao: Writing – review & editing, Supervision, Project administration, Methodology, Investigation. Yuhuan Wang: Data curation, Investigation, Validation, Writing – review & editing.

#### **Declaration of Competing Interest**

The authors declare that they have no known competing financial interests or personal relationships that could have appeared to influence the work reported in this paper.

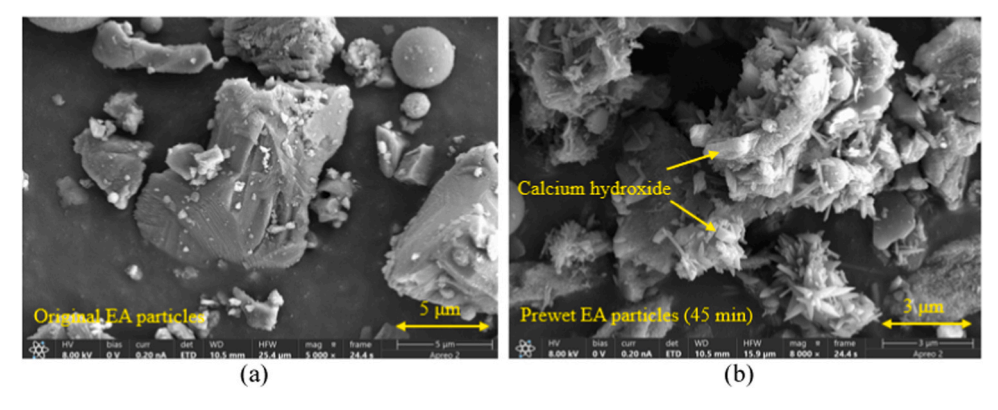


Fig. 18. SEM images of the original EA particles and prewet EA particles.

#### **Data Availability**

Data will be made available on request.

#### Acknowledgement

This research is supported by the National Science Foundation [grant number CMMI-2046407]. The authors also would like to thank Lehigh Hanson for the donation of Type I cement and slag.

#### Appendix

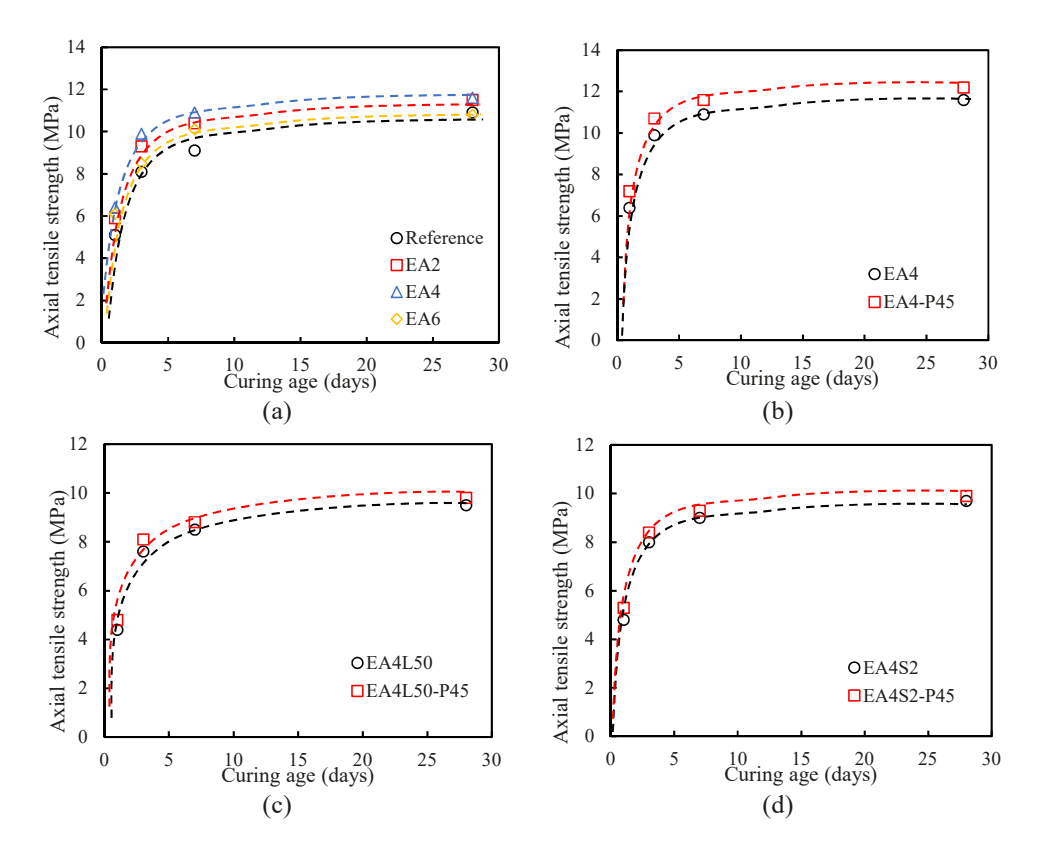


Fig. A1. Experimental and predicting results of axial tensile strength of investigated UHPC.

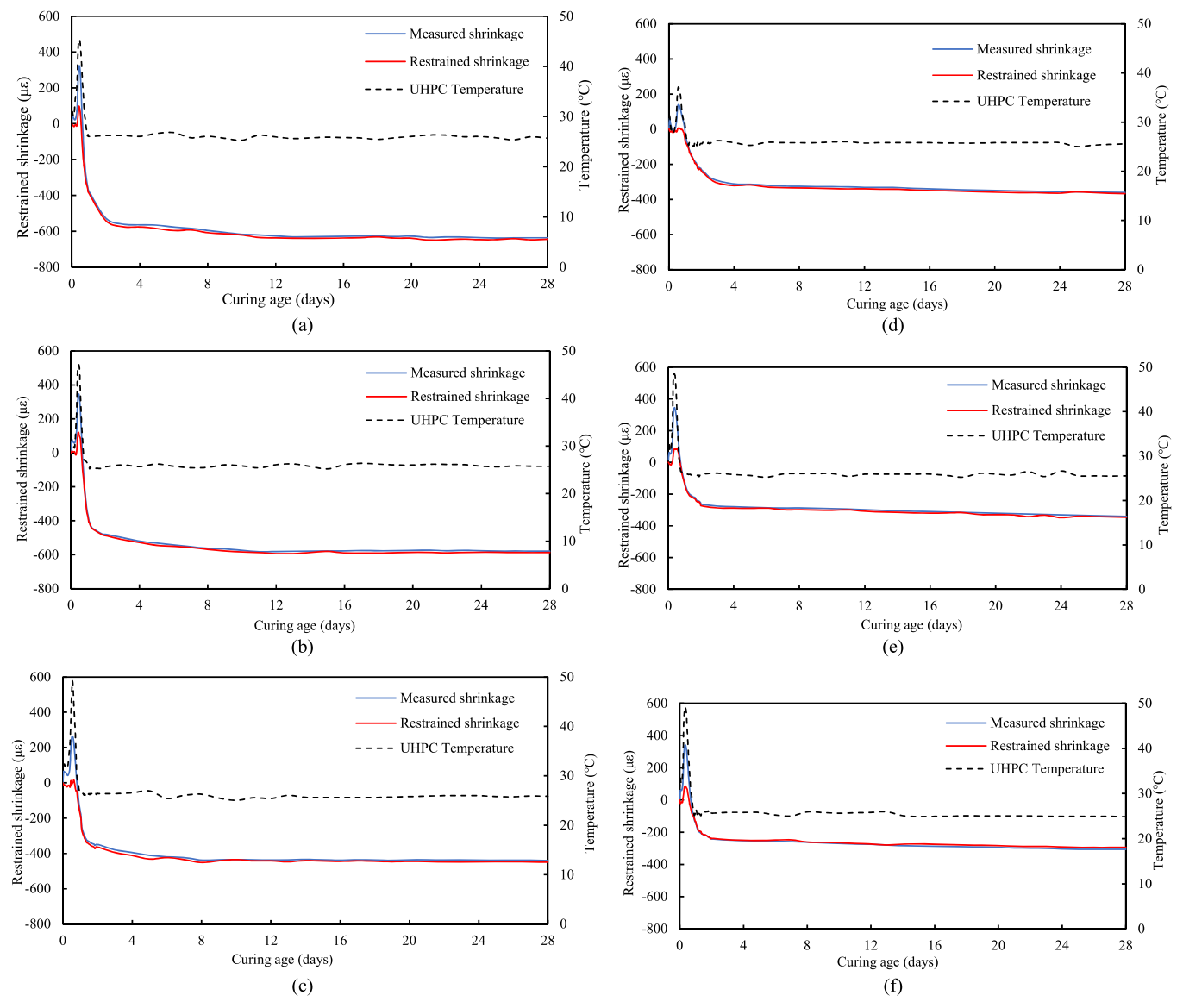


Fig. A2. Results of restrained shrinkage of investigated UHPC mixtures: (a) EA4; (b) EA4-P45; (c) EA4L50; (d) EA4L50-P45; (e) EA4S2; (f) EA4S2-P45.

#### References

- W. Meng, K.H. Khayat, Effects of saturated lightweight sand content on key characteristics of ultra-high-performance concrete, Cem. Concr. Res. 101 (2017) 46–54.
- [2] J. Du, W. Meng, K.H. Khayat, Y. Bao, P. Guo, Z. Lyu, A. Abu-obeidah, H. Nassif, H. Wang, New development of ultra-high-performance concrete (UHPC), Compos. Part B: Eng. (2021) 109220.
- [3] T. Alahmari, C. Kennedy, A. Cuaron, B. Weldon, D. Jauregui, Field testing of a prestressed concrete bridge with high performance and locally developed ultrahigh performance girders, Front. Built Environ. 5 (2019) 114.
- [4] Aaleti, S., Sritharan, S. and Abu-Hawash, A. Innovative UHPC-normal concrete composite bridge deck. in Proceedings of the RILEM-fib-AFGC International Symposium on Ultra-High Performance Reinforced Concrete, Eds: F. Toutlemonde, J. Resplendino, Rilem Publications SARL, Bagneux, France. 2013.
- [5] Voort, T.V, Suleiman, M.T. and Sritharan, S., Design and performance verification of ultra-high performance concrete piles for deep foundations. 2008, Iowa State University. Center for Transportation Research and Education.
- [6] J. Qi, Y. Bao, J. Wang, L. Li, W. Li, Flexural behavior of an innovative dovetail UHPC joint in composite bridges under negative bending moment, Eng. Struct. 200 (2019) 109716.
- [7] Graybeal, B., Field-cast UHPC connections for modular bridge deck elements. 2010.
- [8] Graybeal, B.A., Ultra-high performance concrete composite connections for precast concrete bridge decks. 2012, United States. Federal Highway Administration. Office of Infrastructure Research and Development.

- [9] S. Verger-Leboeuf, J.-P. Charron, B. Massicotte, Design and behavior of UHPFRC field-cast transverse connections between precast bridge deck elements, J. Bridge Eng. 22 (7) (2017) 04017031.
- [10] J. Xie, Q. Fu, J.-B. Yan, Compressive behaviour of stub concrete column strengthened with ultra-high performance concrete jacket, Constr. Build. Mater. 204 (2019) 643–658.
- [11] Haber, Z.B., Munoz, J.F. and Graybeal, B.A., Field testing of an ultra-high performance concrete overlay. 2017, United States. Federal Highway Administration. Office of Infrastructure ....
- [12] Khayat, K.H. and Valipour, M., Design of ultra high performance concrete as an overlay in pavements and bridge decks. 2014, Missouri University of Science and Technology. Center for Transportation Infrastructure and Safety.
- [13] Z.B. Haber, J.F. Munoz, De la Varga, I.and Graybeal, B. A. Bond characterization of UHPC overlays for concrete bridge decks: laboratory and field testing, Constr. Build. Mater. 190 (2018) 1056–1068.
- [14] Wibowo, H. and Sritharan, S., Use of Ultra-High-Performance Concrete for Bridge Deck Overlays. 2018, United States. Federal Highway Administration.
- [15] J. Du, P. Guo, Z. Liu, W. Meng, Highly thixotropic ultra-high-performance concrete (UHPC) as an overlay, Constr. Build. Mater. 366 (2023) 130130.
- [16] Y. Zou, J. Jiang, J. Yang, Z. Zhang, J. Guo, Enhancing the toughness of bonding interface in steel-UHPC composite structure through fiber bridging, Cem. Concr. Compos. 137 (2023) 104947.
- [17] J. Yang, R. Chen, Z. Zhang, Y. Zou, J. Zhou, J. Xia, Experimental study on the ultimate bearing capacity of damaged RC arches strengthened with ultra-high performance concrete, Eng. Struct. 279 (2023) 115611.

- [18] J. Yang, J. Xia, Z. Zhang, Y. Zou, Z. Wang, J. Zhou, Experimental and Numerical Investigations on the Mechanical Behavior of Reinforced Concrete Arches Strengthened with UHPC Subjected to Asymmetric Load. Structures, Elsevier,
- [19] Z. Zhang, K. Pang, L. Xu, Y. Zou, J. Yang, C. Wang, The bond properties between UHPC and stone under different interface treatment methods, Constr. Build. Mater. 365 (2023) 130092.
- [20] J.-Y. Wang, C. Bian, R.-C. Xiao, B. Ma, Restrained shrinkage mechanism of ultra high performance concrete, KSCE J. Civ. Eng. 23 (10) (2019) 4481-4492.
- [21] H. Huang, G. Ye, Examining the "time-zero" of autogenous shrinkage in high/ultrahigh performance cement pastes, Cem. Concr. Res. 97 (2017) 107-114.
- [22] Y. Yang, R. Sato, K. Kawai, Autogenous shrinkage of high-strength concrete containing silica fume under drying at early ages, Cem. Concr. Res. 35 (3) (2005)
- [23] A.K. Cheung, C.K. Leung, Shrinkage reduction of high strength fiber reinforced cementitious composites (HSFRCC) with various water-to-binder ratios, Cem. Concr. Compos. 33 (6) (2011) 661-667.
- [24] J. Du, S. Mahjoubi, Y. Bao, N. Banthia, W. Meng, Modeling mixing kinetics for large-scale production of Ultra-High-Performance Concrete: effects of temperature, volume, and mixing method, Constr. Build. Mater. 397 (2023) 132439
- T.R. Schmitt, D. Darwin, Effect of material properties on cracking in bridge decks, J. Bridge Eng. 4 (1) (1999) 8–13.
- [26] L. Yang, C. Shi, Z. Wu, Mitigation techniques for autogenous shrinkage of ultrahigh-performance concrete-a review, Compos. Part B: Eng. 178 (2019) 107456.
- [27] W. Meng, M. Valipour, K.H. Khayat, Optimization and performance of costeffective ultra-high performance concrete, Mater. Struct. 50 (1) (2017) 29.
- [28] R. Yu, P. Spiesz, H. Brouwers, Development of an eco-friendly Ultra-High Performance Concrete (UHPC) with efficient cement and mineral admixtures uses, Cem. Concr. Compos. 55 (2015) 383-394.
- [29] J. Du, Z. Liu, C. Christodoulatos, M. Conway, Y. Bao, W. Meng, Utilization of offspecification fly ash in preparing ultra-high-performance concrete (UHPC): Mixture design, characterization, and life-cycle assessment, Resour., Conserv. Recycl. 180 (2022) 106136.
- [30] W. Meng, K.H. Khayat, Effect of hybrid fibers on fresh properties, mechanical properties, and autogenous shrinkage of cost-effective UHPC, J. Mater. Civ. Eng. 30 (4) (2018) 04018030.
- [31] C. Wang, C. Yang, F. Liu, C. Wan, X. Pu, Preparation of ultra-high performance concrete with common technology and materials, Cem. Concr. Compos. 34 (4) (2012) 538-544.
- [32] A. Soliman, M. Nehdi, Effects of shrinkage reducing admixture and wollastonite microfiber on early-age behavior of ultra-high performance concrete, Cem. Concr. Compos. 46 (2014) 81-89.
- [33] T. Xie, C. Fang, M.M. Ali, P. Visintin, Characterizations of autogenous and drying shrinkage of ultra-high performance concrete (UHPC); an experimental study. Cem. Concr. Compos. 91 (2018) 156-173.
- [34] J. Justs, M. Wyrzykowski, D. Bajare, P. Lura, Internal curing by superabsorbent oolymers in ultra-high performance concrete, Cem. Concr. Res. 76 (2015) 82–90.
- [35] M. Valipour, K.H. Khayat, Coupled effect of shrinkage-mitigating admixtures and saturated lightweight sand on shrinkage of UHPC for overlay applications, Constr. Build Mater 184 (2018) 320-329
- £361 P. Shen, L. Lu, Y. He, F. Wang, J. Lu, H. Zheng, S. Hu, Investigation on expansion effect of the expansive agents in ultra-high performance concrete, Cem. Concr. Compos. 105 (2020) 103425.
- [37] S. Zhutovsky, K. Kovler, A. Bentur, Effect of hybrid curing on cracking potential of high-performance concrete, Cem. Concr. Res. 54 (2013) 36-42.
- L. Yang, C. Shi, Z. Wu, Mitigation techniques for autogenous shrinkage of ultra-
- high-performance concrete—a review, Compos. Part B Eng. (2019) 107456. [39] L. Liu, Z. Fang, Z. Huang, Y. Wu, Solving shrinkage problem of ultra-highperformance concrete by a combined use of expansive agent, super absorbent polymer, and shrinkage-reducing agent, Compos. Part B Eng. 230 (2022) 109503.
- [40] J.-J. Park, D.-Y. Yoo, S.-W. Kim, Y.-S. Yoon, Benefits of using expansive and shrinkage-reducing agents in UHPC for volume stability, Mag. Concr. Res. 66 (14) (2014) 745-750.
- [41] R. Polat, R. Demirboğa, F. Karagöl, The effect of nano-MgO on the setting time, autogenous shrinkage, microstructure and mechanical properties of high performance cement paste and mortar, Constr. Build. Mater. 156 (2017) 208-218.
- [42] P. Yan, X. Qin, The effect of expansive agent and possibility of delayed ettringite formation in shrinkage-compensating massive concrete, Cem. Concr. Res. 31 (2) (2001) 335-337.
- [43] M. Wyrzykowski, G. Terrasi, P. Lura, Expansive high-performance concrete for chemical-prestress applications, Cem. Concr. Res. 107 (2018) 275-283.
- [44] D.-Y. Yoo, S. Kim, J.-Y. Lee, I. You, S.-J. Lee, Implication of calcium sulfoaluminate-based expansive agent on tensile behavior of ultra-higherformance fiber-reinforced concrete, Constr. Build. Mater. 217 (2019) 679-693.
- [45] S. Anshuang, Q. Ling, Z. Shoujie, Z. Jiayang, L. Zhaoyu, Effects of shrinkage reducing agent and expansive admixture on the volume deformation of ultrahigh performance concrete, Adv. Mater. Sci. Eng. 2017 (2017).
- [46] P. Shen, J.-X. Lu, H. Zheng, L. Lu, F. Wang, Y. He, S. Hu, Expansive ultra-high performance concrete for concrete-filled steel tube applications, Cem. Concr. Compos. 114 (2020) 103813.

- [47] D.-Y. Yoo, J.-J. Kim, B. Chun, Dynamic pullout behavior of half-hooked and twisted steel fibers in ultra-high-performance concrete containing expansive agents, Compos. Part B: Eng. 167 (2019) 517-532.
- [48] L. Teng, A. Addai-Nimoh, K.H. Khayat, Effect of lightweight sand and shrinkage reducing admixture on structural build-up and mechanical performance of UHPC, J. Build. Eng. 68 (2023) 106144.
- [49] W. Meng, K. Khayat, Effects of saturated lightweight sand content on key characteristics of ultra-high-performance concrete, Cem. Concr. Res. 101 (2017)
- [50] ASTM C138 / C138M-17a, Standard Test Method for Density (Unit Weight), Yield, and Air Content (Gravimetric) of Concrete. 2017, ASTM International.
- [51] ASTM C230, Standard Specification for Flow Table for Use in Tests of Hydraulic Cement. 2021, ASTM International.
- [52] ASTM C109 / C109M-20b, Standard Test Method for Compressive Strength of Hydraulic Cement Mortars. 2020, ASTM International.
- M. Jo, L. Soto, M. Arocho St, J. John, S. Hwang, Optimum mix design of fly ash geopolymer paste and its use in pervious concrete for removal of fecal coliforms and phosphorus in water, Constr. Build. Mater. 93 (2015) 1097–1104.
- ASTM C496, Standard Test Method for Splitting Tensile Strength of Cylindrical Concrete Specimens. 2017, ASTM International.
- [55] D. Wanasinghe, F. Aslani, G. Ma, Effect of water to cement ratio, fly ash, and slag on the electromagnetic shielding effectiveness of mortar, Constr. Build. Mater. 256 (2020) 119409.
- [56] D.-Y. Yoo, N. Banthia, Y.-S. Yoon, Effectiveness of shrinkage-reducing admixture in reducing autogenous shrinkage stress of ultra-high-performance fiber-reinforced concrete, Cem. Concr. Compos. 64 (2015) 27–36.
- Jonasson, J.-E. Slipform construction-calculations for assessing protection against early freezing. Publication of: Cement and Concrete Research Institute. 1984, (4.84).
- O. Linderoth, L. Wadsö, D. Jansen, Long-term cement hydration studies with isothermal calorimetry, Cem. Concr. Res. 141 (2021) 106344.
- R. Yang, R. Yu, Z. Shui, X. Gao, X. Xiao, X. Zhang, Y. Wang, Y. He, Low carbon design of an ultra-high performance concrete (UHPC) incorporating phosphorous slag, J. Clean. Prod. 240 (2019) 118157.
- Oliva, M.G. and Cramer, S. Self-consolidating concrete: creep and shrinkage characteristics. Report, University of Wisconsin. 2008.
- E.-i Tazawa, Autogenous Shrinkage of Concrete, CRC Press, 1999.
- [62] M. Yan, X. Tan, S. Mahjoubi, Y. Bao, Strain transfer effect on measurements with distributed fiber optic sensors, Autom. Constr. 139 (2022) 104262.
- [63] Mahjoubi, S., Tan, X. and Bao, Y. Inverse analysis of strain distributions sensed by distributed fiber optic sensors subject to strain transfer. Mechanical Systems and Signal Processing. In Press .
- X. Tan, L. Fan, Y. Huang, Y. Bao, Detection, visualization, quantification, and warning of pipe corrosion using distributed fiber optic sensors, Autom. Constr. 132 (2021) 103953.
- [65] Holt, E.E., Early age autogenous shrinkage of concrete. 2001: University of Washington.
- D.Y. Yoo, J.J. Park, S.W. Kim, Y.S. Yoon, Influence of reinforcing bar type on autogenous shrinkage stress and bond behavior of ultra high performance fiber reinforced concrete, Cem. Concr. Compos. 48 (2014) 150-161.
- S. Shivakumar, M. Qin, D. Zhang, C. Hu, Q. Yan, J. Luo, A new type of compositionally complex M5Si3 silicides: Cation ordering and unexpected phase stability, Scr. Mater. 212 (2022) 114557.
- [68] G.H. Tattersall, Workability and quality control of concrete, CRC Press, 1991.
- [69] P. Guo, J. Du, Y. Bao, W. Meng, Real-time video recognition for assessing plastic viscosity of ultra-high-performance concrete (UHPC), Measurement 191 (2022) 110809.
- [70] J. Du, P. Guo, W. Meng, Effect of water-based nanoclay and ambient temperature on rheological properties of UHPC pastes, Constr. Build. Mater. 370 (2023) 130733
- [71] S. Li, S. Cheng, L. Mo, M. Deng, Effects of Steel Slag Powder and Expansive Agent on the Properties of Ultra-High Performance Concrete (UHPC): Based on a Case Study, Materials 13 (3) (2020) 683.
- Z. Pan, Y. Zhu, D. Zhang, N. Chen, Y. Yang, X. Cai, Effect of expansive agents on the workability, crack resistance and durability of shrinkage-compensating concrete with low contents of fibers, Constr. Build. Mater. 259 (2020) 119768.
- [73] M.S. Meddah, M. Suzuki, R. Sato, Influence of a combination of expansive and shrinkage-reducing admixture on autogenous deformation and self-stress of silica fume high-performance concrete, Constr. Build. Mater. 25 (1) (2011) 239-250.
- [74] H. Shuguang, L. Yue, Research on the hydration, hardening mechanism, and microstructure of high performance expansive concrete, Cem. Concr. Res. 29 (7) (1999) 1013-1017.
- [75] D.-Y. Yoo, J.-J. Park, S.-W. Kim, Y.-S. Yoon, Early age setting, shrinkage and tensile characteristics of ultra high performance fiber reinforced concrete, Constr. Build. Mater. 41 (2013) 427-438.
- D. Shen, J. Kang, Y. Jiao, M. Li, C. Li, Effects of different silica fume dosages on early-age behavior and cracking resistance of high strength concrete under restrained condition, Constr. Build. Mater. 263 (2020) 120218.
- Z. Liu, J. Du, W. Meng, Achieving low-carbon cementitious materials with high mechanical properties using CaCO3 suspension produced by CO2 sequestration, J. Clean. Prod. 373 (2022) 133546.